Check for updates

Development of bimetallic nickel-based catalysts supported on activated carbon for green fuel production†

Wan Nor Adira Wan Khalit,[abc] Tengku Sharifah Marliza,[*ac] N. Asikin-Mijan, [ID][d] M. Safa Gamal,[ab] Mohd Izham Saiman,[ab] Mohd Lokman Ibrahim[ef] and Y. H. Taufiq-Yap [ID] [*abg]

In this work, the catalytic deoxygenation of waste cooking oil (WCO) over acid–base bifunctional catalysts (NiLa, NiCe, NiFe, NiMn, NiZn, and NiW) supported on activated carbon (AC) was investigated. A high hydrocarbon yield above 60% with lower oxygenated species was found in the liquid product, with the product being selective toward n-(C_{15} + C_{17})-diesel fractions. The predominance of n-(C_{15} + C_{17}) hydrocarbons with the concurrent production of CO and CO_2, indicated that the deoxygenation pathway proceeded *via* decarbonylation and decarboxylation mechanisms. High deoxygenation activity with better n-(C_{15} + C_{17}) selectivity over NiLa/AC exposed the great synergistic interaction between La and Ni, and the compatibility of the acid–base sites increased the removal of oxygenated species. The effect of La on the deoxygenation reaction performance was investigated and it was found that a high percentage of La species would be beneficial for the removal of C–O bonded species. The optimum deoxygenation activity of 88% hydrocarbon yield with 75% n-(C_{15} + C_{17}) selectivity was obtained over 20% of La, which strongly evinced that La leads to a greater enhancement of the deoxygenation activity. The NiLa/AC reusability study showed consistent deoxygenation reactions with 80% hydrocarbon yield and 60% n-(C_{15} + C_{17}) hydrocarbon selectivity within 6 runs.

1. Introduction

Environmental pollution and the depletion of fossil fuel have become twin crises in the world today. The burning of fossil fuels has contributed to an increase in carbon dioxide (CO_2) levels in the atmosphere, which simultaneously increased the average temperature of the earth.[1,2] Currently, fossil fuels supply 80% of the world's energy demand, and about 90% of the total supply is utilized in the transportation sector, thus, worsening the atmospheric pollution. To overcome these problems, the exploitation of alternate biofuels from non-fossil sources such as animal fats, vegetable oils and algae has become the focus.[3,4] Recently, biomass-derived triglyceride-based feedstocks such as vegetable oils have gained significant attention as sustainable biodiesel feedstock due to their great abundance, easy availability and low cost.[5,6] However, biodiesel has its drawbacks such as higher viscosity, rich oxygen content, high unsaturated acid content and low volatility.[7,8] Higher oxygen contents cause severe engine problems like carbon deposit and lubricant thickening.[9] Hence, there is a strong need to find other alternatives that have similar properties to petroleum fuel to replace transesterification technology such as the deoxygenation reaction for green diesel production.

Biofuel known as green diesel consists of straight-chain hydrocarbon C_{12}–C_{20} that can be derived from triglycerides *via* the catalytic deoxygenation process: (i) decarboxylation (–CO_2) and (ii) decarbonylation (–CO, H_2O) (deCOx). These methods need thermal energy with a compatible catalyst to remove the oxygenated species from the feedstock in a H_2-free environment. Commonly, the obtained green diesel is virtually identical to conventional diesel; *e.g.*, the amount of oxygen is close to zero after the elimination of oxygen in terms of CO, CO_2 and H_2O.[10–12]

aCatalysis Science and Technology Research Centre (PutraCat), Faculty of Science, Universiti Putra Malaysia, 43400 UPM Serdang, Selangor, Malaysia. E-mail: taufiq@upm.edu.my; Fax: +60-3-89466758; Tel: +60-3-89466809

bDepartment of Chemistry, Faculty of Science, Universiti Putra Malaysia, 43400 UPM Serdang, Selangor, Malaysia

cDepartment of Science and Technology, Universiti Putra Malaysia Bintulu Campus, Nyabau Road, 97008 Bintulu, Sarawak, Malaysia. E-mail: t_marliza@upm.edu.my; Fax: +60-86-855428; Tel: +60-86-855430

dDepartment of Chemical Sciences, Faculty of Science and Technology, Universiti Kebangsaan Malaysia, 43600 UKM Bangi, Selangor Darul Ehsan, Malaysia

eSchool of Chemistry and Environment, Faculty of Applied Sciences, Universiti Teknologi MARA (UiTM), 40450 Shah Alam, Selangor, Malaysia

fCentre of Nanomaterials Science, Institute of Science, Universiti Teknologi MARA (UiTM), 40450 Shah Alam, Selangor, Malaysia

gChancellery Office, Universiti Malaysia Sabah, 88400 Kota Kinabalu, Sabah, Malaysia

† Electronic supplementary information (ESI) available. See DOI: 10.1039/d0ra06302a

The excessive production of waste cooking oil (WCO) has become a serious global concern. The European Union (EU) produces approximately 700 000–1 000 000 tonnes of WCO annually.[13] The WCO production in Asian countries, *e.g.*, China, Indonesia, Malaysia, *etc.*, and the Special Administrative Region (SAR), *e.g.*, Taiwan and Hong Kong, is estimated to be 40 000 tonnes per year.[14,15] Improper WCO disposal could increase the levels of organic pollutants in the land and water which leads to environmental pollution.[16] The proper recycling of WCO by converting to industrial products such as green diesel is considered to be an ideal solution.

Several catalysts like Pt/C, Pd/C, Ni/C, Ni–Co/MWCNT, Ni/MgO and ReNiMo/γ-Al$_2$O$_3$ have been extensively investigated for the catalytic deoxygenation of various feedstocks.[17–20] According to Morgan and co-workers,[17] they found that the deoxygenation of triolein, tristearin and soybean oil can be done over Pt/C, Pd/C and 20Ni/C catalysts; the 20Ni/C catalyst yielded over 80% of C$_8$–C$_{17}$ fractions. Zulkepli *et al.*[21] confirmed that the deoxygenation of triolein over Ni promoted catalysts could result in the diesel products of (n-(C$_{11}$–C$_{20}$)). They suggested that the Ni promoter consists of acidic sites that increase the promotion of C–C and C–O bond cleavage and render high yields of diesel fractions. However, strong acidic sites of Ni may result in the formation of severe catalyst deactivators such as coke.[22]

The accumulation of active species caused by carbon deposition on a catalyst support also favours the migration of metallic particles to produce larger aggregates, resulting in poor dispersity, thereby decreasing the deoxygenation activity.[23–25] Interestingly, the incorporation of a coke inhibitor species (base or acid–base metal promoter) such as La, Fe, and Zn forming a binary system could reduce the deactivation rate.[26–28] It was suggested that the synergistic interaction of the acid and basic sites originating from those metal species could promote greater catalyst stability and enhance deoxygenation activity. Instead of a base or acid–base promoter, the use of an acidic metal such as Ce, Mn, and W has been reported to be catalytically effective in promoting C–O bond cleavage activity, and some of these metals have also been shown to be good coke-suppressing agents. Coa and co-workers[29] revealed that ∼5.5% of coke was formed on the CeO$_2$/SBA-15 catalyst in the deoxygenation of WCO. Moreover, the high removal of oxygenating activity was also observed in the pyrolysis of microalgae oil (*Tetraselmis* sp. and *Isochrysis* sp.) over Ni–Ce/Al$_2$O$_3$ and Ni–Ce/ZrO$_2$ catalyst and implied that the oxidative properties of CeO$_2$ play a critical role in improving the reaction activity.[30–33] Ce can also form reducible oxides that can simply gasify the carbon deposition due to its redox properties (Ce^{3+}/Ce^{4+}).[34–36] There have been several reports on the enhancement of the deoxygenation activity over W–CaO and Mn-based catalysts and these metals also exhibited promising deoxygenation performances.[37,38]

Besides the metal promoters, the catalyst support also plays a major role in improving the deoxygenation of oxygenated species. Recently, some studies have focused on the deoxygenation of assorted feedstocks over a variety of carbon-supported catalysts.[38–40] It appears that the use of activated carbon (AC) could inhibit coke formation and simultaneously enhance the spent catalyst life. Abdulkareem-alsultan *et al.*[28] reported the high stability of Ag$_2$O$_3$–La$_2$O$_3$/AC with consistent deoxygenation for six runs. Similar trends also have been observed by the same researchers in the deoxygenation of WCO over CaO–La$_2$O$_3$/AC, high hydrocarbon yield (>72%), and n-C$_{15}$ selectivity (>80%) was performed within six runs and coke formed was less than 2 wt%.[41] Due to the advantages of AC and the unique properties of binary metal promoters, the present study is focused on the development of a series of binary metal oxides (NiLa, NiFe, NiZn, NiW, NiCe, and NiMn) supported on AC catalysts for the deoxygenation of WCO under a H$_2$-free atmosphere. The outcomes of the nature of the binary metal oxides on maintaining high catalytic activity are also elucidated.

2. Experimental

2.1 Materials

Commercial activated carbon (AC) derived from charcoal was obtained from Fluka. Sulfuric acid (H$_2$SO$_4$) was procured from USA (J.T.Baker) (95–98 wt% purity). Nickel(II) nitrate hexahydrate (Ni(NO$_2$)$_3$·6H$_2$O) with 99.0% purity and cerium(III) nitrate hexahydrate (CeN$_3$O$_9$·6H$_2$O) with 99.5% purity were obtained from Acros. Lanthanum(III) nitrate hydrate (La(NO$_3$)$_3$·xH$_2$O) with 99.9% purity, ammonium metatungstate hydrate ((NH$_4$)$_6$W$_{12}$O$_{39}$·xH$_2$O) with ≥85.0% purity, zinc nitrate hexahydrate (N$_2$O$_6$Zn·6H$_2$O) with 98.0% purity, and alkane and alkene standards n-(C$_8$–C$_{20}$) (with purity >98%) were obtained from Sigma Aldrich. Ferric nitrate nonahydrate (Fe(NO$_3$)$_3$·9H$_2$O) with 98.0% purity was procured from Systerm, and manganese(II) acetate tetrahydrate (C$_4$H$_6$MnO$_4$·4H$_2$O) with 99.0% purity was obtained from R&M Chemical company. The GC grade n-hexane (with purity >98%) was purchased from Merck. The feedstock for this study was WCO, which was directly used without further treatment and was kindly supplied by a restaurant in Universiti Putra Malaysia, Serdang, Selangor Malaysia. Table 1 summarizes the chemical properties of the crude WCO.

2.2 Synthesis of catalysts

Binary metal oxides supported on AC catalysts were synthesized *via* a wet impregnation process. Firstly, 7 g of commercial AC was activated by reflux with 95 mL of concentrated H$_2$SO$_4$ at 150 °C for 12 h, then it was washed with warm water until the pH of 7 was achieved. The resulting material was filtered and dried at 100 °C for 12 h. The respective aqueous Ni salt (20 wt%) and Fe salt (20 wt%) were further impregnated on AC surfaces under constant stirring for 12 h and directly dried overnight at 100 °C. The resulting solid was ground and calcined at 700 °C for 4 h under a N$_2$ environment. This method was adapted from Aliana-Nasharuddin *et al.* with slight modification.[42] The same procedure was applied to the impregnation of AC with a constant amount of 20 wt% of Ni, Ce, Fe, Mn, La, W and Zn salts. The catalysts were designated as NiFe/AC, NiCe/AC, NiMn/AC, NiLa/AC, NiW/AC and NiZn/AC.

Table 1 Property evaluation of WCO as green diesel feedstock

Properties	Standard methods	WCO
FFA content (%)	—	13.9
Acid value (mg KOH g^{-1})	ASTM D974	27.8
Fatty acid composition[a] (%)		
Myristic acid (C14)		4.5
Palmitic acid (C16)		22.0
Stearic acid (C18:0)		2.1
Oleic acid (C18:1)		48.1
Linoleic acid (C18:2)		7.6
Gadoleic acid (C20:1)		13.0
Others[b]		2.7

[a] GC programs: column: zebron ZB5 ms (30 m × 0.25 mm I.D. × 0.25 μm); temperature program: starting from 50 °C and hold for three min before heating to 300 °C at 10 °C min^{-1}. GCMS detector and injector temperature: 250 °C; flow rate: 1 mL min^{-1}; carrier gas: helium. [b] Others = $C_{11}H_{20}O$, $C_{21}H_{42}O_2Si$ and $C_{30}H_{50}$, $C_{26}H_{50}$.

2.3 Characterization of catalysts

The crystallography of the prepared mixed metal oxide supported AC catalysts was determined using the Shimadzu XRD-6000 X-ray Diffractometer (XRD). The scan range was set from 2° to 80°, assisted by Cu K$_\alpha$ radiation ($\lambda = 0.15406$ nm, 40 kV, 30 mA).

The Thermo-Finnigan Shopmatic 1990 series N$_2$ sorption analyser was used to determine the specific surface area and pore distribution by using the Brunauer–Emmett–Teller (BET) and Barrett–Joyner–Halenda (BJH) technique. Initially, the catalysts were degassed for 12 h at 150 °C to eliminate impurities and moisture on the catalyst surface. The adsorption and desorption processes of N$_2$ were evaluated in a vacuum chamber at −196 °C. The morphological analysis and the elemental analysis of the prepared catalyst were investigated using A LEO 1455 VP FESEM equipped with a Rayny EDX-720 energy dispersive X-ray spectrometer. The EDX analyser was launched to determine the composition of Ni, Fe, Ce, Mn, La, W, Ni, Zn, and C on the catalyst surface.

The acidity and basicity of the prepared catalysts were analysed using a Thermo-Finnigan TPD/R/O 1100 instrument equipped with a thermo-conductivity detector (TCD); temperature-programmed desorption – ammonia (TPD-NH$_3$) and temperature-programmed desorption – carbon dioxide (TPD-CO$_2$). For acidity determination, about ~0.05 g of the catalyst was pre-treated with N$_2$ gas for 45 min at 150 °C, and the adsorption of NH$_3$ gas on the surface of the catalyst was continued for one hour. After that, the overloaded NH$_3$ gas was removed with N$_2$ gas at a flow rate of 20 mL min^{-1}. Finally, the analysis was started during the heating of the sample from 50 °C to 950 °C with helium gas flow (30 mL min^{-1}); the desorption of NH$_3$ gas from the acidic sites of the catalysts was identified by TCD. The same technique was used to analyse the basicity of the catalyst with CO$_2$ as the probe gas replacing the NH$_3$ gas.

Thermal analysis of the catalyst was carried out using a TGA/DSC 1 Mettler Toledo thermogravimetric analyser. The sample was heated from 50 °C to 1000 °C at a heating rate of 15 °C min^{-1} in a N$_2$ environment to determine the stability of the catalyst, and in an O$_2$ environment to determine coke formation.

2.4 The catalytic deoxygenation reaction of WCO

The catalytic deoxygenation reaction of 10 g WCO was conducted in a 250 mL autoclave semi-batch reactor, containing 3 wt% catalyst, and the reactor was flushed with N$_2$ gas to let out the O$_2$ molecules in the system. This technique was adapted from Abdulkareem-Alsultan et al.[28] The reactor was then heated to 350 °C, and the stirring was adjusted to 300 rpm and maintained for 2 h with 50 mL min^{-1} of N$_2$ flow. During the reaction, the condensable products were condensed from the reactor via a cold trap with a temperature of 20 °C, and the liquid products were collected and analysed using an Agilent Technologies 7890 A Gas chromatography-flame ionization detector (GC-FID) and SHIMADZU model QP2010 Plus Gas chromatography-mass spectroscopy (GC-MS). To trap the gases released, a Tedlar gas bag was used after 1 h of reaction and subsequently analysed by using GC with thermal conductivity detector (GC-TCD).

2.5 Liquid products analysis

An Agilent Technologies 7890 A GC-FID was used to quantitatively analyse the products; the alkane and alkene standards n-(C$_8$–C$_{20}$) and 1-bromohexane were used as the internal standards. The GC was equipped with an HP-5 capillary column (30 m × 0.32 mm × 0.25 μm) with helium gas as the carrier gas. Prior to analysis, a 2.0 μL aliquot of the deoxygenated liquid product was introduced into the GC injector port at 250 °C. The initial oven temperature was set at 40 °C and held for 6 min, then it was ramped up to 270 °C at the heating rate of 7 °C min^{-1}. The total hydrocarbon yield (Y) was determined as the summation of the peak areas of alkanes and alkenes in the range of n-(C$_8$–C$_{20}$) as shown in (eqn (1)), where A_a denotes the total peak area of alkanes, A_e denotes the total peak area of alkenes, and $\sum A_p$ denotes the total peak area for all the deoxygenized and non-deoxygenized products.[43]

$$Y = (\textstyle\sum A_a + \sum A_e)/(\sum A_p) \times 100\% \qquad (1)$$

The selectivity for the hydrocarbons (HC) was determined by eqn (2), where A_h denotes the total peak area of the selected hydrocarbon, and A_t is the total area of hydrocarbons detected in the liquid product.[42]

$$HC = (A_h/(\textstyle\sum A_t)) \times 100\% \qquad (2)$$

A SHIMADZU model QP2010 Plus GC-MS with a non-polar Zebron ZB5 ms column (30 m × 0.25 mm I.D. × 0.25 μm) with a splitless inlet was used to qualitatively investigate the WCO and deoxygenated liquid products. Briefly, the samples were diluted to 100 ppm with high-purity (>98%) GC-grade hexane. The resulting peaks observed in the GC spectrum were analysed using the National Institute of Standards and Testing Library (NIST)

and the main products were matched with probabilities exceeding 95%. The gas product was analysed using an Agilent USA Model G1540 N system with a thermal conductivity detector (TCD). About 0.20 mL of the collected gas in the Tedlar bag was introduced into the gas chromatograph. Standard gases such as CO_2, H_2, CO, and CH_4 were used to calibrate the yields of collected gases. The gas products were split using He as the carrier gas. The collected gases were calculated and compared with the percentage of the standard gas.

Furthermore, the Perkin Elmer Spectrum (PS) 100 FT-IR was used to study the functional groups of the liquid products operating in the range of 300–4000 cm^{-1} with a resolution of 4 cm^{-1}.

3.   Results and discussion

The XRD patterns of the AC and catalysts of the binary metal oxide-supported AC are shown in Fig. 1. The XRD of the treated AC exhibited an amorphous structure with a wide hump at $2\theta = 20.28°–28.70°$ along with intense diffraction peaks at $2\theta = 44.60°$, $64.68°$, and $77.55°$, which are likely attributed to C.[44] The presence of the amorphous carbon structure is evidence of the randomly oriented carbon sheets and this ensures that all catalysts have a high content of non-graphitic carbon in their structure. The intensity of the broad hump disappeared after it was impregnated with the active metals, suggesting the intercalation of metals implanted on the AC and the metal were successfully introduced in the support.[44] Hence, it was suggested that the active metals promoted greater dispersion on the AC.

It was observed that most of the binary metal oxide supported ACs showed the formation of the cubic metallic Ni^0 at 2θ

$= 44.51°$. In the case of NiW/AC and NiZn/AC, they showed the additional appearance of cubic NiO at $2\theta = 37.44°$, $43.47°$, $63.20°$, and $75.37°$, which suggest that the lattice oxygen in W and Zn-containing catalysts possess low redox ability.[45] The successful incorporation of La, W, Ce, Fe, Zn, and Mn on Ni/AC was evinced by the formation of the XRD diffraction peaks for the hexagonal structure of La_2O_3, cubic CeO_2, tetragonal W_4O_{11}, hexagonal ZnO, and cubic MnO. Besides, NiFe/AC and NiW/AC showed the presence of the bimetallic phase for $NiFe_2O_4$, NiFe and $NiWO_4$. However, in the case of the NiFe/AC catalyst, it was observed that the diffraction peak belonging to cubic metallic Ni^0 slightly shifted from $2\theta = 44.51°$ to $44.01°$ due to the addition of Fe atoms to the crystal lattice of Ni, and resulted in the formation of the NiFe alloy phase at $2\theta = 51.29°$ and $75.34°$ as shown in Fig. 1e. This finding is in agreement with studies by Chen *et al.* and Li *et al.*, where they reported that when Fe was added to the lattice of Ni, it caused deformation in the catalyst crystallinity and the formation of the NiFe alloy, which also resulted in the shifting of the diffraction peak of Ni^0 in $Ni_{0.9}Fe_{0.1}$–Cr_2O_3 and Ni_3Fe_1/CeO_2 catalysts to lower angles.[46,47] It was also suggested that some of the Ni atoms were bonded to the Fe and W atoms by oxygen-bridged bonds to form Ni–Fe and Ni–W composite oxides. It is worth mentioning that the diffraction peak intensity of ZnO increased remarkably with the loading of NiO. This shows that the addition of NiO may promote the migration of ZnO crystallites to grow into larger particles, which is aligned with the report by Li *et al.*[48]

The specific surface area and pore volume of the catalysts were determined using the BET and BJH methods, and the results are tabulated in Table 2. It was noted that the AC had the highest surface area of 869 m^2 g^{-1}, and this was gradually decreased to the range of 130–485 m^2 g^{-1} after the
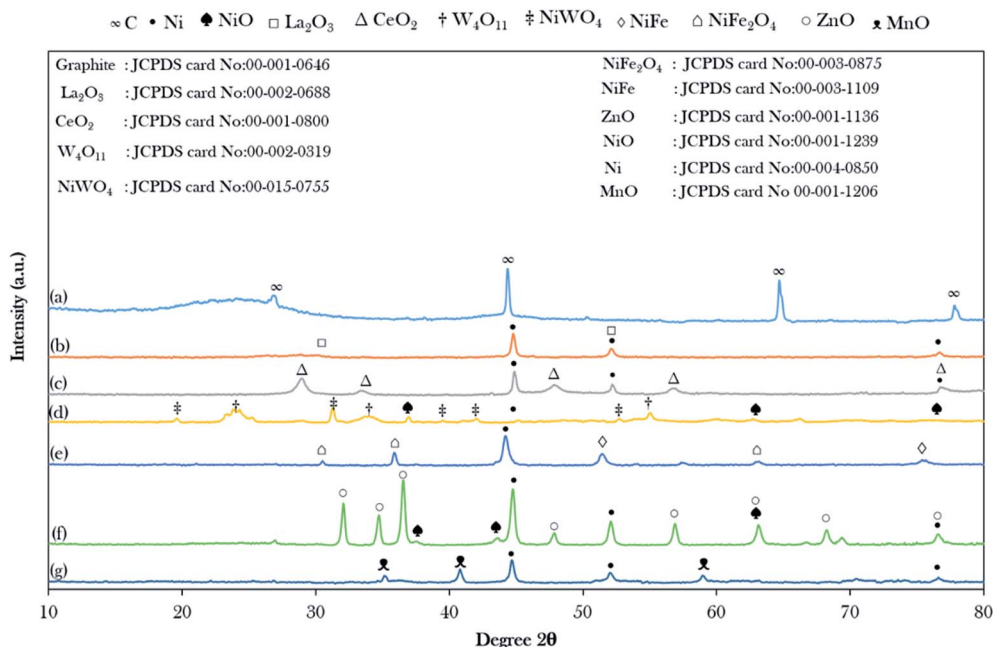

Fig. 1   X-ray diffractograms of the binary metal oxide-supported AC: (a) activated carbon (AC), (b) NiLa/AC, (c) NiCe/AC, (d) NiW/AC, (e) NiFe/AC, (f) NiZn/AC and (g) NiMn/AC.

Table 2 Physicochemical properties of the binary metal oxide-supported AC

Catalysts	N$_2$ adsorption–desorption analysis			TPD-NH$_3$[c]			TPD-CO$_2$[d]		
	Surface area[a] (m^2 g^{-1})	Pore size diameter[b] (nm)	Pore volume[b] (cm^3 g^{-1})	T (°C)	Amount of NH$_3$ adsorbed (µmol g^{-1})	Total number of acidic sites (µmol g^{-1})	T (°C)	Amount of CO$_2$ adsorbed (µmol g^{-1})	Total number of basic sites (µmol g^{-1})
AC	869	3.24	0.70	—	—	—	—	—	—
NiLa/AC	336	3.62	0.30	635	2192	2192	637	799	799
NiCe/AC	380	8.67	0.10	568/699	1180/2081	3261	694	627	627
NiW/AC	130	2.78	0.09	958	18 068	18 068	853/952	1584/2093	3677
NiFe/AC	441	3.62	0.40	778	5981	5981	788	2541	2541
NiZn/AC	446	3.34	0.37	650/834	781/7034	7815	579/808	53/3123	3176
NiMn/AC	485	3.08	0.37	479/643	408/1226	1634	573/647/950	48/236/2017	2301

[a] Measured by BET analysis. [b] Measured by BJH analysis. [c] Determined by TPD-NH$_3$ analysis. [d] Determined by TPD-CO$_2$ analysis.

incorporation of active metals. This trend was in good agreement with another study that claimed that the reduction of the surface area was due to the successful impregnation of metal oxides on the surface of the AC support.[49] The NiW/AC showed the lowest surface area of 130 m^2 g^{-1}, which might be due to the aggregation of W on the surface of AC that blocked the pores.[50] This finding was strongly evinced by the remarkable reduction in the pore diameter and pore volume for NiW/AC, while the
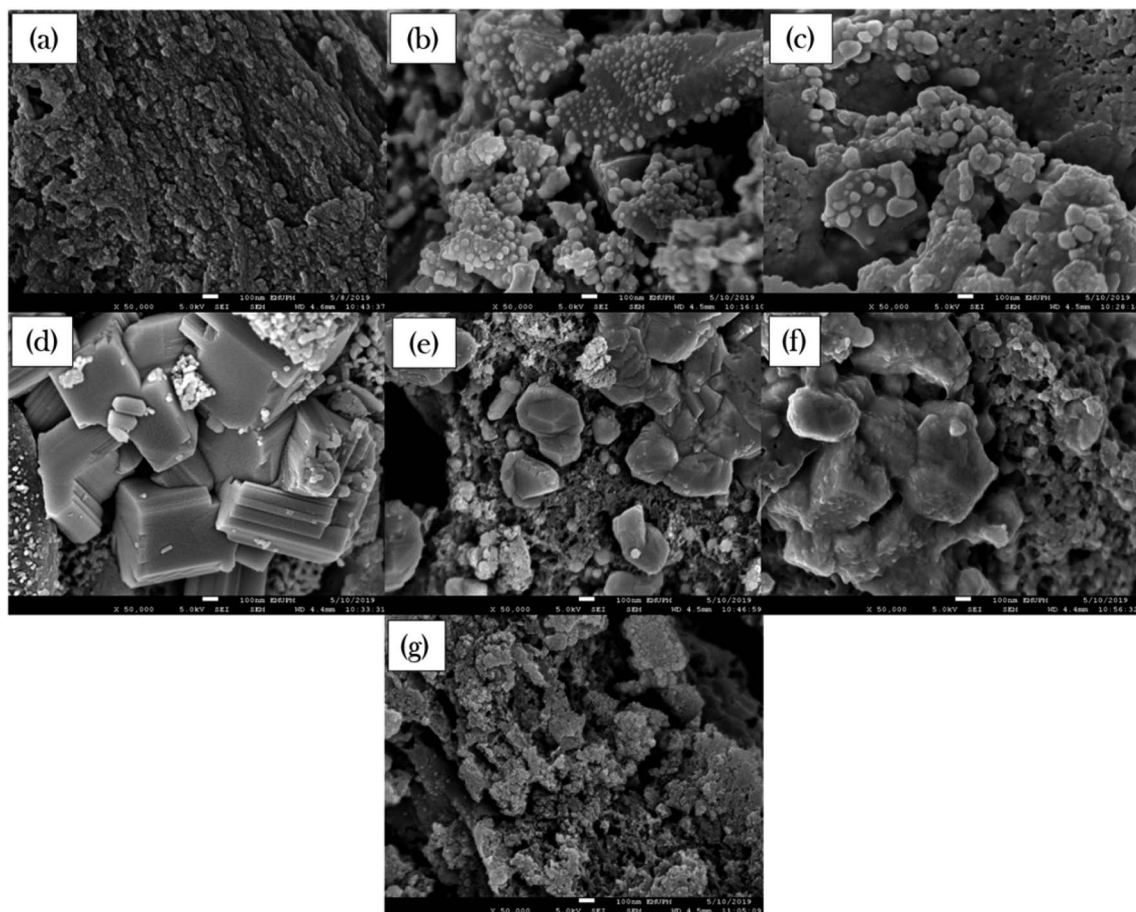

Fig. 2 FESEM images of (a) AC, (b) NiLa/AC, (c) NiCe/AC, (d) NiW/AC, (e) NiFe/AC, (f) NiZn/AC and (g) NiMn/AC. (Magnifications ×50 000).

Table 3 Elemental compositions of binary metal oxide-supported AC catalysts

| Catalysts | Elemental surface analysis (wt%) | | | | | | | | |
	C	O	Ni	La	Ce	W	Fe	Zn	Mn
AC	76.7	23.3	—	—	—	—	—	—	—
NiLa/AC	56.6	19.1	9.0	15.4	—	—	—	—	—
NiCe/AC	49.6	18.8	16.7	—	14.8	—	—	—	—
NiW/AC	56.5	14.3	4.0	—	—	25.0	—	—	—
NiFe/AC	63.1	23.8	7.0	—	—	—	6.1	—	—
NiZn/AC	73.0	16.3	5.5	—	—	—	—	4.9	—
NiMn/AC	76.4	13.1	4.7	—	—	—	—	—	5.8

pore diameter and pore volume of AC were remarkably reduced from 3.24 nm to 2.78 nm and 0.70 cm^3 g^{-1} to 0.09 cm^3 g^{-1}, respectively. Notably, indistinguishable pore diameter changes of less than 10% pore enlargement were observed for the prepared metal-loaded ACs; however, the NiCe/AC showed 62% enlargement in pore diameter. Similar findings were observed for NiCe/HZSM-5 by Balasundram and co-workers, where the pore size diameter of NiCe/HZSM-5 was remarkably enlarged when compared to the unmodified support HZSM-5.[29,51] One can see that the Ce species rendered greater pore enlargement outcomes. It was reported that large pore systems may not beneficial for deoxygenation as it may induce high aromatization reactions.[52]

The surface morphology and elemental composition of all binary metal oxide-supported AC catalysts were studied by FESEM-EDX and the results are presented in Fig. 2 and Table 3, respectively. The external surface topographies of the metal-supported AC were found to vary with the dense rough surface of the AC support. The FESEM images of NiLa/AC and NiCe/AC (Fig. 2b and c) show the formation of the rough surface morphology decorated by well-developed tiny dots. In contrast, NiW/AC, NiFe/AC, and NiZn/AC displayed the formation of compact bulk structures (Fig. 2d–f). It was also worth noticing that NiW/AC also had a large cubic shape with a smooth surface belonging to W (Fig. S1†), while the NiMn/AC showed a slight agglomeration of particles.

Theoretically, clear morphological changes in the textural morphology of AC after the addition of the active metal can be ascribed to dopant effects resulting in aggregation. The EDX analysis revealed that all the binary metal oxide-supported AC catalysts were comprised mainly of C species, which covered about 49–78 wt% from the total weight of the sample. Therefore, all of these catalysts are expected to have excellent mechanical properties during catalytic deoxygenation activity and thus increase the catalyst stability and catalytic activity.[53,54] The C content was gradually reduced upon the incorporation the metals due to the addition of binary metals on the AC support.[44] Overall, the elemental composition of active metal was slightly below the expected value (20 wt%) due to the major active metals being deposited within the interior of the AC support,[55] which can be seen from the reduction in the pore volume in Table 2.

The density, distribution and strength of the active sites of the catalysts were investigated using TPD-NH$_3$ and TPD-CO$_2$ for acidic and basic properties, respectively, as shown in Fig. 3 and Table 2. It was observed that the desorption of NH$_3$ and CO$_2$ started at temperatures above 500 °C, indicating that all of the catalysts exhibited strongly acidic and strongly basic sites.[50] The trend in the acid strength of catalysts is as follows: NiW/AC > NiZn/AC > NiFe/AC > NiCe/AC > NiLa/AC > NiMn/AC. The highest strength was demonstrated by the NiW/AC catalyst with a total acidity of 18 068 μmol g^{-1}. According to Asikin-Mijan et al., Janampelli, and Darbha, the large total acidity is due to the characteristics of the W metal.[37,56] The Ni–Zn containing catalyst also has a high acidic density of 7815 μmol g^{-1} of active sites, which can be explained by the Ni–O–Zn domains and coordinatively unsaturated Ni^{2+} in the AC-supported catalyst (Fig. 1).

The total densities of the basic sites of prepared catalysts are of the following order: NiW/AC > NiZn/AC > NiFe/AC > NiMn/AC > NiLa/AC > NiCe/AC. The W-containing catalyst also has the highest basic density and strength, which deviates from the high acidic characteristics of W. This finding implies that the modification of Ni/AC with W can establish new acid–base properties.[37] Overall, all binary metal oxide catalysts display acid–base properties; hence, it could be expected that these
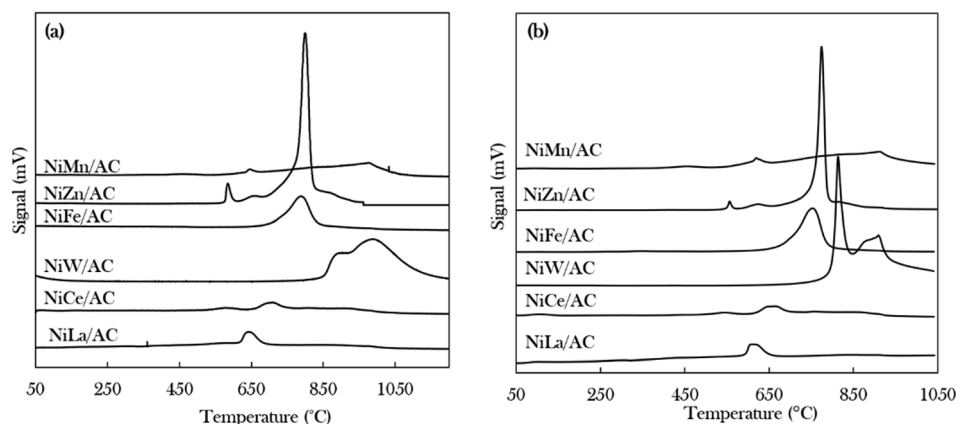
Fig. 3 Temperature-programmed desorption patterns of (a) TPD-NH$_3$ and (b) TPD-CO$_2$ of binary metal oxide-supported AC catalysts.
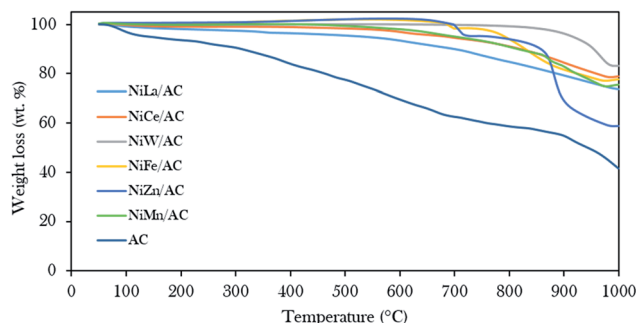
Fig. 4 Thermal gravimetric analysis profiles of the prepared AC and binary metal oxide-supported AC catalysts.

catalysts would have the ability to remove oxygenated species *via* cracking and deCOx routes.

Fig. 4 displays the thermal stability profiles for AC and binary metal oxide-supported AC catalysts. The results revealed that AC rendered three stages of weight loss: 100–200 °C, 210–420 °C, and 430–850 °C. The beginning weight loss was assigned to the loss of H_2O molecules at about 6.7 wt%,[31,42,57] the second weight loss was associated with the decomposition of cellulose at about 11.2 wt% and the third major weight loss was about 40.5 wt%, due to the decomposition of carbonaceous compounds.[58,59] In contrast to binary metal oxide-supported AC catalysts, a minor weight loss of less than 35 wt% due to carbonaceous materials was observed at decomposition temperatures above 600 °C. This finding proves that the presence of metal oxides on AC as support gives significant thermodynamic stability to the parent AC.[44]

3.1 Deoxygenation activity of WCO

The deoxygenation process of WCO was conducted with a catalyst loading of 3 wt%, a reaction time of 2 h and reaction temperature of 350 °C, with stirring speed of 300 rpm in an inert N_2 flow system. The hydrocarbon yield (%) and product selectivity (%) are summarized in Fig. 5. The results showed the increment in the hydrocarbon yield in the following order:

blank < AC < NiW/AC < NiMn/AC < NiFe/AC < NiCe/AC < NiLa/AC < NiZn/AC. The blank test showed that the reaction was hardly taking place at 350 °C, which contributed to the hydrocarbon yield of only ~12%. Similar behaviour was observed for the AC-catalysed deoxygenation; only 37% of the hydrocarbon yield was achieved.

However, all the prepared binary mixed metal oxide-supported AC catalysts resulted in remarkably higher hydrocarbon (C_8–C_{20}) yields >75%, and only NiW/AC gave 60%. This implies that the acid–base properties were responsible for the efficient subtraction of the oxygen-bonded species reaction. According to Asikin-Mijan *et al.* active sites could accelerate the cracking activity and thus result in the formation of rich light gaseous compounds.[37] This discovery is in line with the results of Roussel *et al.*, who showed that the employment of NiW/silica–alumina in the hydrocracking of *n*-decane also resulted in the formation of linear C_2 alkanes.[60]

Notably, NiZn/AC exhibited the highest hydrocarbon yield at 92%. This indicates that the presence of Ni–O–Zn, along with the presence of acid–base sites in NiZn/AC, was very effective in transforming the WCO to oxy-free hydrocarbon compounds.[61] In the case of hydrocarbon selectivity, the blank test and AC-catalysed deoxygenation formed major light fractions of *n*-C_8 to *n*-C_{14} with a total selectivity of about 55–66%. With the addition of active metals, the light fractions decreased to 25–37%, and the desired deCOx product *n*-(C_{15} + C_{17}) increased remarkably to >58%. Among the binary metal oxide-supported catalysts, NiLa/AC showed the highest *n*-(C_{15} + C_{17}) selectivity (76%), while NiCe/AC had the lowest (58%). The lowest *n*-(C_{15} + C_{17}) selectivity by NiCe/AC strongly affirmed that the significantly large pores structures (8.67 nm as shown in Table 2) retarded the C–O bond cleavage activity. This result was in accordance with the results of Twaiq *et al.* who implied that large pore structured catalysts are capable of increasing the propensity for cracking activity and result in lower *n*-(C_{15} + C_{17}) selectivity.[62] Given this, it is suggested that the pore size structure is also a critical factor in determining the deCOx reaction. It is worth noting that the changes in the surface area had no effect on the *n*-(C_{15} + C_{17}) selectivity.
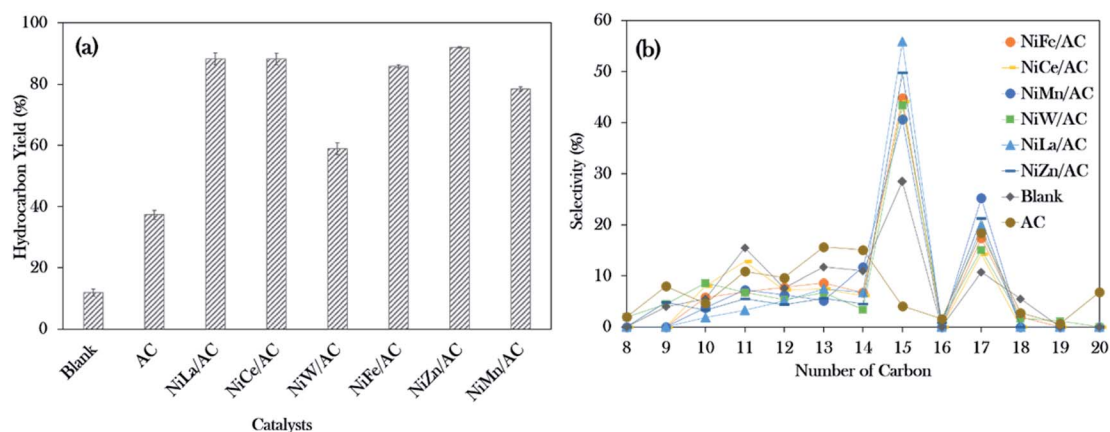

Fig. 5 Data collected from the deoxygenation process: (a) hydrocarbon yield and (b) *n*-(C_{15} + C_{17}) selectivity for blank and catalysed deoxygenation (operating parameters: 3 wt% of catalyst loading, 350 °C reaction temperature, 2 h reaction time under inert conditions).

Referring to the acid–base properties of the catalysts in Table 2, it was observed that the deCOx activity was limited by catalysts with higher concentrations of strong acid sites. This was revealed by the n-(C_{15} + C_{17}) output, which was lowered over NiMn/AC at only 66%.

The GCMS results of the product distribution in Fig. 6a show that the total distribution of the n-(C_8–C_{20}) deoxygenated liquid catalysed by AC and binary mixed metal oxide-supported AC catalysts was in the range of 65% to 81%. The catalyst performance was of the following order arrangement: NiZn/AC > NiCe/AC > NiLa/AC = NiFe/AC > NiW/AC > NiMn/AC > AC. It can be concluded that the total hydrocarbon distribution determined by GC-FID was slightly higher as compared to the GCMS results. This is due to the presence of the hydrocarbon isomer compounds (Z) and (E), such as 5-undecene (E)- and 3-hexadecene (Z)-.[41] The isomeric compounds are commonly developed from the isomerization of alkenes; the higher isomer compounds (9.88%) were obtained over NiFe/AC catalyst, due to the Fe-promoted catalyst capable of motivating the isomerization reaction.[63]

NiMn/AC exhibited the highest ketone product by 16%, due to the greater numbers of basic sites than acidic sites in the catalyst, which resulted in the increment of the ketonization rate.[37,64,65] It was also said that the ketonization is not favourable when the catalyst co-exists with a large number of acid sites. Although the NiW/AC and NiZn/AC catalysts had the highest concentrations of basic sites (>3000 μmol g⁻¹), the smallest amounts of ketone compounds were detected (0–1%) for both

catalysts. It was further discovered that both catalysts were rich in acidic sites (>7000 μmol g⁻¹).

Cycloalkanes such as cyclopentadecane and n-nonylcyclohexane were increased for NiLa/AC-catalysed deoxygenation, resulting in total cyclic compounds of about 21%. Li et al. reported that the La-containing catalyst favoured cyclization and aromatization reactions forming monocyclic aromatic hydrocarbons.[66] It was noted that the NiLa/AC rendered side reactions; however, it was still considered to be very effective to the drive deoxygenation activity, exclusively via the deCOx reaction.

Fourier transform infrared (FTIR) spectra were used to analyse the functional groups of the deoxygenated liquid products as exhibited in Fig. 6b. It was found that the primary absorption bands of WCO were at 1120 cm⁻¹, 1740 cm⁻¹, and 2922 cm⁻¹, and these were attributed to the carbonyl group (C–O–C), the ester group (C=O), and the stretching absorption of the C–H bond, respectively.[67] It also showed that the deoxygenated liquid products rendered a carboxylic acid (–COOH) group peak at 1711 cm⁻¹, indicating that the deoxygenation of WCO was initiated by breaking the ester bond of triglycerides. The successful progression of deoxygenation activity was also in accordance with the disappearance of the carbonyl group (C–O–C) absorption band at 1120 cm⁻¹. This resulted in correspondence with Gamal et al.[44] who proposed that the occurrence of deoxygenation activity showed the reduction of intensities in the C=O group and C–O absorption bands as compared to feedstock. However, Satyarthi and Srinivas[68] reported that the
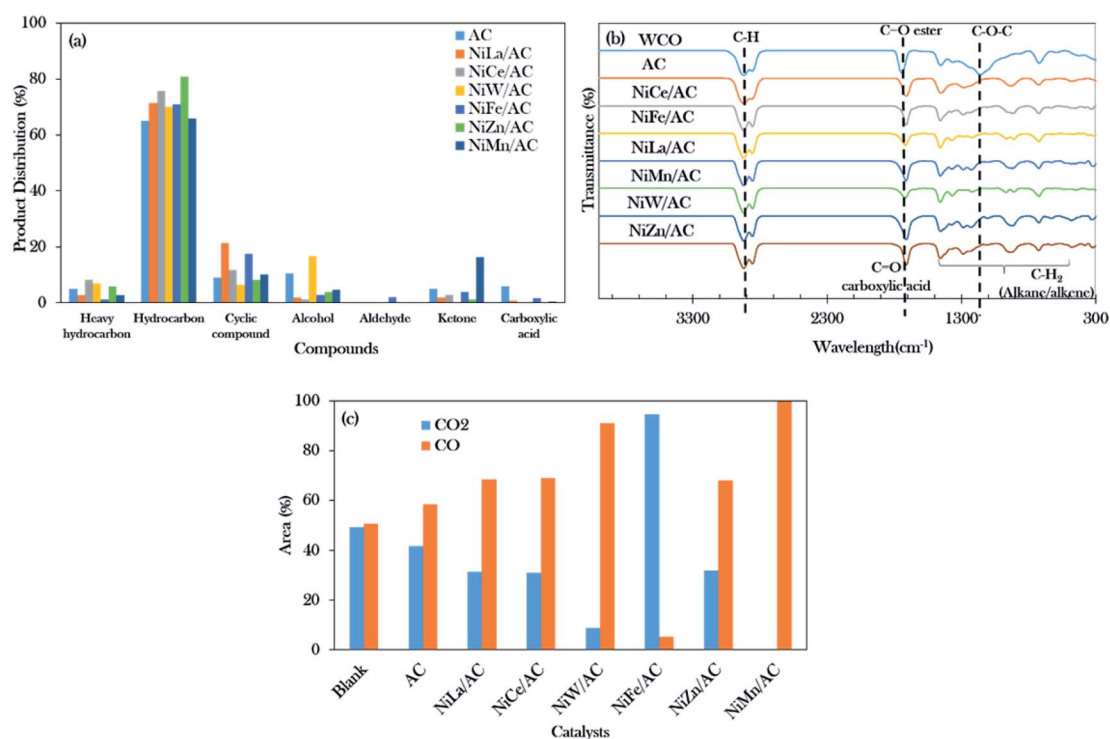

Fig. 6 Data collected from liquid deoxygenized liquid products: (a) product distribution, (b) FTIR spectra of the WCO and deoxygenized liquid product catalysed by AC and binary mixed oxide-supported AC (c) the compositions of CO_2 and CO gases over catalytic deoxygenation (operating parameters: 3 wt% of catalyst loading, 350 °C reaction temperature, 2 h reaction time under inert conditions).

characteristics of the C–H stretching absorption peak (2922 cm^{-1}) could not affect the formation of *n*-alkanes.

Moreover, Fig. 6c shows the composition analyses of CO_2 and CO gases collected from the reaction process. Theoretically, the deoxygenation of WCO in the absence of H_2 will favour the decarboxylation and decarbonylation reactions and produce carbon gases such as CO_2 and CO.[44] The CO gas predominates in the majority of the binary metal oxide-supported AC catalysed reactions except for NiFe/AC. The results showed that the deoxygenation reaction of WCO over NiLa/AC, NiCe/AC, NiW/AC, NiZn/AC, and NiMn/AC followed decarbonylation pathways, while NiFe/AC favoured decarboxylation pathways.

A mechanism was proposed for the catalytic deoxygenation of WCO over Ni-based catalysts (Fig. 7). Table 1 shows that WCO contains palmitic acid, C_{16} (22%), and oleic acid, C_{18} (48%), fatty acids. The catalytic deoxygenation reaction of WCO *via* the decarbonylation and decarboxylation (deCOx) pathway resulted in C_{n-1} hydrocarbon formation (C_{15} and C_{17}) and by-products (CO_2, CO and water). Fig. 7a shows the proposed reaction

pathway for the deoxygenation of oleic acid. Firstly, the double bonds of oleic acid were hydrogenated to produce stearic acid as the intermediate product using *in situ* hydrogen that was generated *via* the water gas shift (WGS) reaction (pathway A).[69,70] Thereafter, the deoxygenation reaction took place through the decarboxylation process by the elimination of O_2 in the form of CO_2, and resulted in *n*-heptadecane ($C_{17}H_{36}$) as the product (pathway B). The decarbonylation reaction directly produced 1-heptadecene ($C_{17}H_{34}$) through the removal of O_2 in the form of CO and H_2O (pathway C). Most of the liquid products produced higher yields of *n*-C_{15}, hence it was proposed that the mild cracking occurred through C–C cleavage from the *n*-C_{17} fraction and produced large amounts of *n*-C_{15} (pathway D). This was in agreement with the results of Aliana-Nashnaruddin *et al.*,[42] who produced high *n*-C_{15} fractions in the catalytic deoxygenation of chicken fat oil.

On the other hand, Fig. 7b shows that the deoxygenation activity of the palmitic acid resulted in *n*-pentadecane ($C_{15}H_{32}$) and 1-pentadecene ($C_{15}H_{30}$) by the decarboxylation and
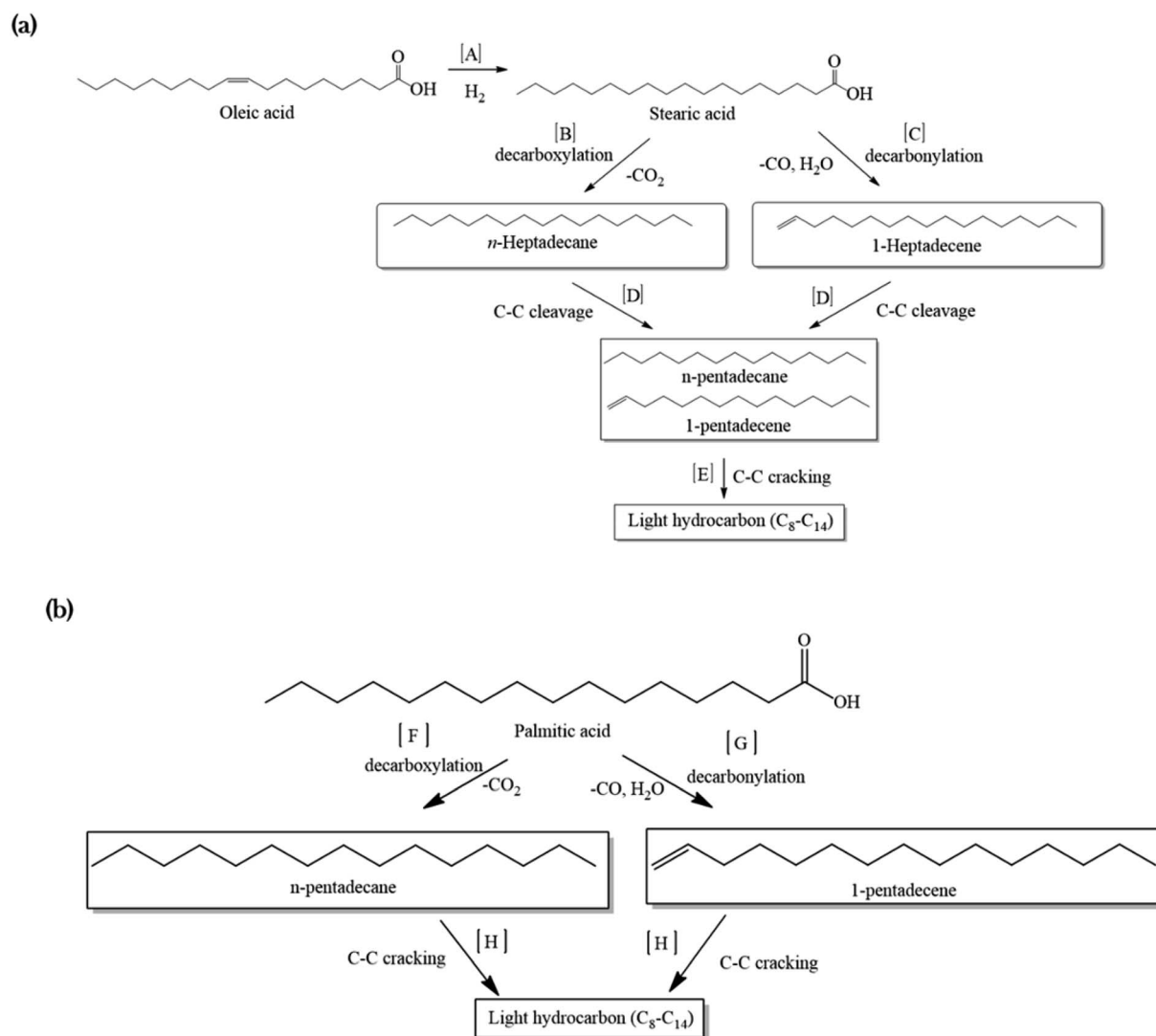

Fig. 7 The proposed reaction mechanism for a Ni-based catalyst in the catalytic deoxygenation of WCO for (a) oleic acid and (b) palmitic acid.

decarbonylation reaction (pathways F and G). Further C–C cracking of liquid products produced light hydrocarbons n-(C$_8$–C$_{14}$) (pathway E and H). The GC-FID results (Fig. 5) showed the formation of light hydrocarbons after the deoxygenation reaction. Hence, it can be concluded that the pathway for the deoxygenation of WCO using NiLa/AC, NiCe/AC, NiW/AC, NiZn/AC, and NiMn/AC catalyst followed the decarbonylation reaction and NiFe/AC favoured the decarboxylation reaction based on the composition of the gases Fig. 6c.

3.2 The effect of La concentration on the deoxygenation of WCO

Based on the primary catalytic screening study (Fig. 5a and b), it was found that NiLa/AC is an effective catalyst as compared to others in the catalytic deoxygenation reaction. Thus, the effect of the La concentration within the range of 5–30% was further studied to identify the concentration of La that would optimise the transformation of WCO to the diesel range under the deoxygenation activity conditions at 350 °C with 3 wt% of catalyst for 2 h reaction time and with a stirring speed of 300 rpm; the data are presented in Fig. 8a. It was found that the binary metal oxide catalyst NiLa/AC had increased the hydrocarbon yield from 75% to 89% as the concentration of La increased from 5% to 25%. However, the yield of hydrocarbon

decreased when the concentration of La increased to 30%. This might be due to the excess La that saturated the surface of AC, covering the active sites of the catalyst.[28]

Fig. 8b shows that the majority of the deoxygenated liquid products were composed of the n-(C$_8$ to C$_{20}$) hydrocarbons. The highest total selectivity of n-(C$_{15}$ + C$_{17}$) followed the order Ni$_{20}$La$_{20}$/AC > Ni$_{20}$La$_{25}$/AC > Ni$_{20}$La$_{10}$/AC > Ni$_{20}$La$_5$/AC > La$_{20}$/AC > Ni$_{20}$La$_{30}$/AC > Ni$_{20}$La$_{15}$/AC. High deCOx activity was observed for the Ni$_{20}$La$_{20}$AC-catalysed deoxygenation, which strongly affirmed that the moderate density of the strongly acidic sites (2192 μmol g^{-1}) and the low density of the strongly basic sites (799 μmol g^{-1}), as shown in Fig. 8c, d and Table 4, were beneficial for the enhancement of the deCOx activity. This finding is also in good agreement with that of Kim et al., where a large number of strongly acidic sites is not preferable to moderate and low amounts of strong acid sites, as this tends to increase the coking activity and deteriorate the catalyst stability.[71] Overall, the moderate acidic strength and its density of Ni$_{20}$La$_{20}$/AC catalyst were attributed to the synergistic effects between the Ni and La$_2$O$_3$ species on the exterior surface of AC, which favoured the deCOx reaction via C–O cleavage and yielded a higher percentage of n-(C$_{15}$ + C$_{17}$) selectivity. Similar findings were observed by Abdulkareem-Alsultan et al.,[28] who showed that the presence of the Ag$_2$O$_{3(10\%)}$–La$_2$O$_{3(20\%)}$/AC$_{nano}$
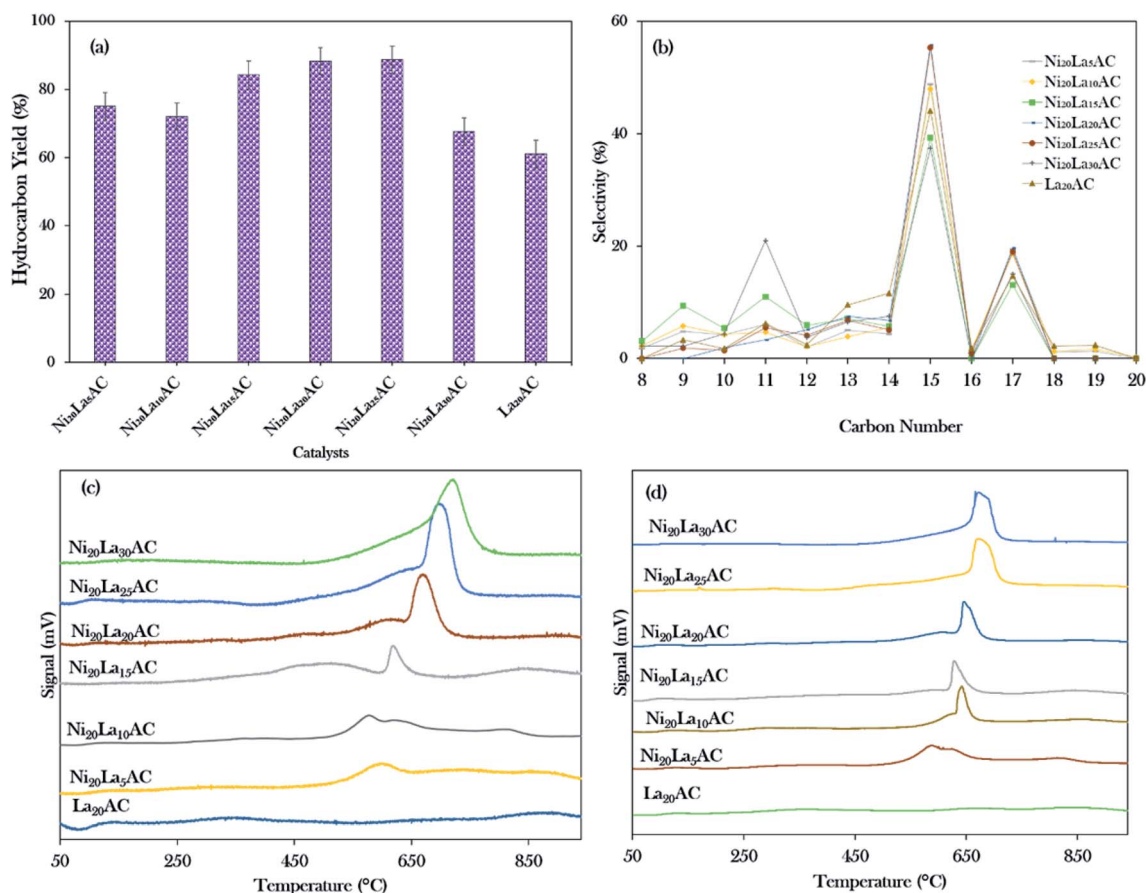

Fig. 8 (a) Hydrocarbon yield, (b) hydrocarbon selectivity, (c) TPD-NH$_3$, (d) TPD-CO$_2$ for the catalytic deoxygenation of WCO over different concentrations of La (5–30 wt%).

Table 4 Acidity and basicity of different La concentrations

Catalysts	TPD-NH$_3$		TPD-CO$_2$	
	Temp. (amount of NH$_3$ adsorbed)	Total number of acidic sites (μmol g^{-1})	Temp. (amount of CO$_2$ adsorbed)	Total number of basic sites (μmol g^{-1})
La$_{20}$AC	338 °C (469 μmol g^{-1}) 890 °C (708 μmol g^{-1})	1177	364 °C (207 μmol g^{-1}) 676 °C (164 μmol g^{-1}) 841 °C (187 μmol g^{-1})	558
Ni$_{20}$La$_5$AC	635 °C (651 μmol g^{-1}) 870 °C (529 μmol g^{-1})	1180	109 °C (46 μmol g^{-1}) 641 °C (599 μmol g^{-1}) 874 °C (532 μmol g^{-1})	1177
Ni$_{20}$La$_{10}$AC	578 °C (1403 μmol g^{-1})	1403	635 °C (1150 μmol g^{-1})	1150
Ni$_{20}$La$_{15}$AC	513 °C (740 μmol g^{-1}) 620 °C (386 μmol g^{-1}) 833 °C (856 μmol g^{-1})	1982	104 °C (59 μmol g^{-1}) 628 °C (461 μmol g^{-1}) 844 °C (631 μmol g^{-1})	1151
Ni$_{20}$La$_{20}$AC	635 °C (2192 μmol g^{-1})	2192	637 °C (799 μmol g^{-1})	799
Ni$_{20}$La$_{25}$AC	696 °C (3799 μmol g^{-1})	3799	672 °C (1184 μmol g^{-1})	1184
Ni$_{20}$La$_{30}$AC	721 °C (3606 μmol g^{-1})	3606	666 °C (1023 μmol g^{-1})	1023

catalyst under a H$_2$-free environment resulted in the greater hydrocarbon yield (~89%) and selectivity for n-(C$_{15}$ + C$_{17}$) (~93%). This also suggested that the rich La$_2$O$_3$ species induced C–O bond breaking. The higher rate of C–O bond breaking over the rich La-containing catalyst is possibly due to the formation of a large quantity of acid–base sites and also the unique characteristics of La$_2$O$_3$ itself.[41,72]

3.3 Optimization of WCO over NiLa/AC catalyst

Based on the initial screening study, the NiLa/AC catalyst was the operative catalyst; hence, the optimization study of the

NiLa/AC (Ni = 20 wt%; La = 20 wt%) catalyst was conducted by the one-variable-at-a-time (OVAT) approach. Three parameters were evaluated, namely, catalyst loading (0.5–7%), reaction time (30–180 min), and reaction temperature (300–400 °C). The effects of catalyst loading on the hydrocarbon yield and the hydrocarbon selectivity were studied at 350 °C, 2 h, and 300 rpm stirring speed in an inert atmosphere. The hydrocarbon yield and hydrocarbon selectivity n-(C$_{15}$ + C$_{17}$) gradually increased from 71% to 88%, and 59% to 75%, respectively, when the catalyst was added to the system from 0.5 wt% to 3 wt%. On the contrary, the hydrocarbon yield and n-(C$_{15}$ + C$_{17}$) selectivity
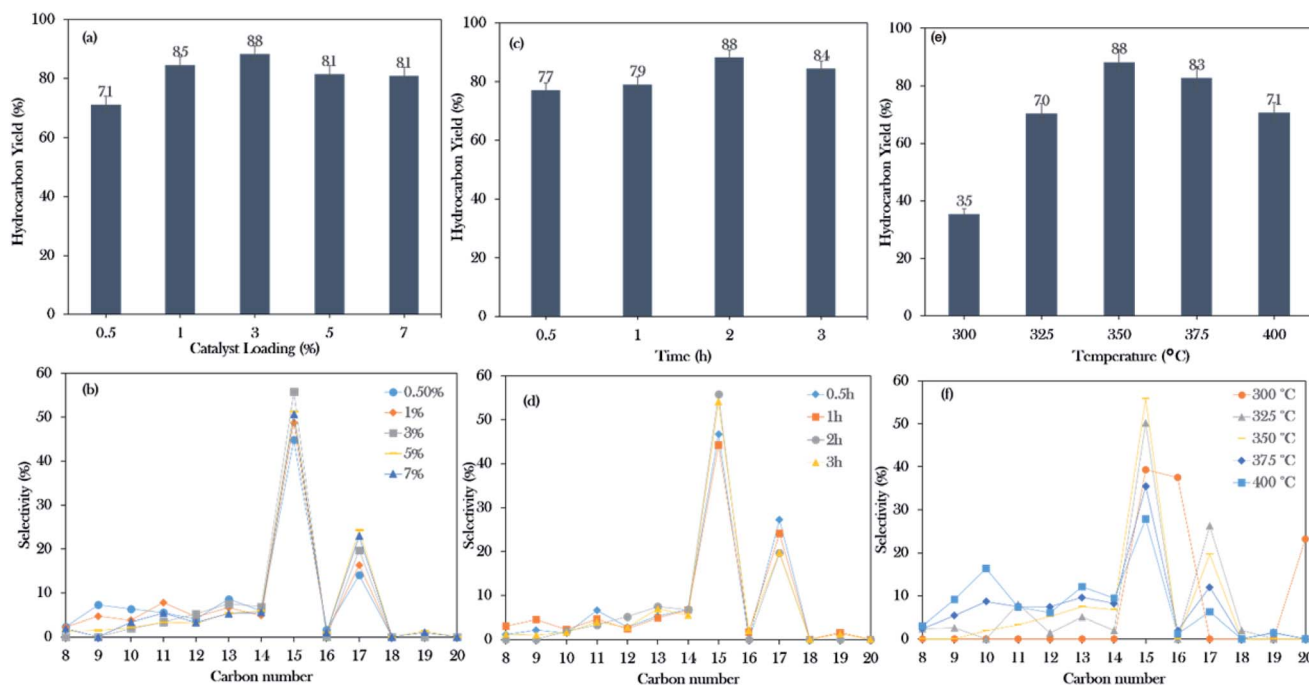

Fig. 9 Optimization studies of WCO: (a and b) the effects of catalyst loading, parameters: 350 °C and 2 h reaction time. (c and d) The effects of reaction time, parameters: 350 °C and 3 wt% catalyst loading. (e and f) The effects of reaction temperature, parameters: 3 wt% catalyst loading and 2 h reaction time with a stirring rate of 300 rpm and under an inert atmosphere.

decreased upon increasing the catalyst loading beyond 5 wt% as shown in Fig. 9a and b. According to Lou et al.,[73] an excess of the active sites could lead to undesired secondary reactions, such as polymerization reactions; therefore, 3 wt% of catalyst loading is preferable for the deoxygenation reaction.

The experiments on the effects of reaction time on deoxygenation reactions were conducted at 350 °C, 3 wt% catalyst loading, and 300 rpm stirring rate in an inert atmosphere. The collected data showed that the hydrocarbon yield gradually increased from 77% to 88% and the hydrocarbon selectivity for $n\text{-}(C_{15} + C_{17})$ increased from 74% to 75% when the time was extended from 30 min to 2 h. Thus, it was suggested that the deoxygenation reaction still occurred for up to 2 h of reaction time. However, it was observed that beyond 3 h of reaction, it only led to a decrease in the hydrocarbon yield to 84% and the $n\text{-}(C_{15} + C_{17})$ selectivity was reduced to 74% (Fig. 9c and d). According to Abdulkareem-Alsultan et al., this was due to the cracking of the deoxygenated liquid product and the increase in the light fraction of hydrocarbons and the consequent production of gaseous products.[41] In this work, the optimum reaction duration was 2 h for an effective deoxygenation reaction.

Moreover, the influence of the temperature on the WCO was determined at 2 h reaction time, 3 wt% catalyst loading, 300 rpm stirring rate in a N_2 atmosphere. Referring to Fig. 9e and f, it was observed that heating the system from 300 to 350 °C could increase the hydrocarbon yield and $n\text{-}(C_{15} + C_{17})$ selectivity from 35–88% and 39–75%, respectively. Interestingly, the percentage of C_{16} and C_{20} fractions was significantly higher at 300 °C, due to the cracking and polymerization reactions that predominantly occurred when the deoxygenation proceeded under mild reaction condition (temperature: 270–400 °C; time: 30–240 min; catalyst loading: 0.5–9%).[41,74] It should be noted that the WCO was mainly comprised of C16:0 and C18:1 (Table 1); rich C_{16} species may also have originated from the cracking of the C18:1 fatty acid, forming the C_{16} fraction. This occurrence is consistent with that of Aliana-Nasharuddin et al.,[42] who suggested in their reaction mechanism scheme that the chicken

fat oil (CFO) was composed mainly of C_{16} and C_{18} fatty acids. When CFO was deoxygenized via the deCOx reaction, it resulted in the formation of C_{15} and C_{17}. Further cracking of C_{18} fatty acids also resulted in the formation of C_{16} fatty acids. In the case of C_{20}, hypothetically, the C_{20} is formed via the polymerization reaction of short-chain hydrocarbons into a longer carbon complex.[18] However, increasing the reaction temperature above 375 °C only reduced the deoxygenation activity. Bernas et al.[75] revealed that the reduction of the deoxygenation activity at high temperature is due to the occurrence of the thermal cracking reaction, which drastically increased the formation of light hydrocarbons in the range of $n\text{-}(C_8\text{-}C_{13})$. In summary, the deoxygenation activity is very sensitive to the heat change, which could significantly affect the hydrocarbon yield and $n\text{-}(C_{15} + C_{17})$. From this finding, 88% hydrocarbon yield and 75% hydrocarbon selectivity $n\text{-}(C_{15} + C_{17})$ were obtained when the reactions were conducted with 3 wt% at the reaction temperature of 350 °C for a reaction time of 2 h.

3.4 The reusability and stability of the NiLa/AC catalyst

Reusability studies of a catalyst are crucial for estimating the economics of the NiLa/AC (Ni = 20 wt%; La = 20 wt%) catalyst for large scale production. The reusability of the catalyst was investigated under the favourable reaction conditions of 3 wt% catalyst loading, 2 h reaction time, 10 g of WCO, and 350 °C. The spent catalyst was reactivated by washing with hexane and it was reused for the next reaction cycle under the same reaction conditions. In this work, the deoxygenation reaction was performed for 6 consecutive runs. Surprisingly, the results revealed that the hydrocarbon yield was maintained over 80% and the hydrocarbon selectivity for $n\text{-}(C_{15} + C_{17})$ was over 60%, as exhibited in Fig. 10a and b. It was concluded that the NiLa/AC catalyst has outstanding mechanical properties and chemical stability. This was supported by XRD patterns for the spent catalyst, where the diffraction peaks of Ni and La_2O_3 for the fresh and spent NiLa/AC remained after 6 consecutive runs (Fig. 11a), meaning that there were no changes in the structural phases of the active metals in each cycle.
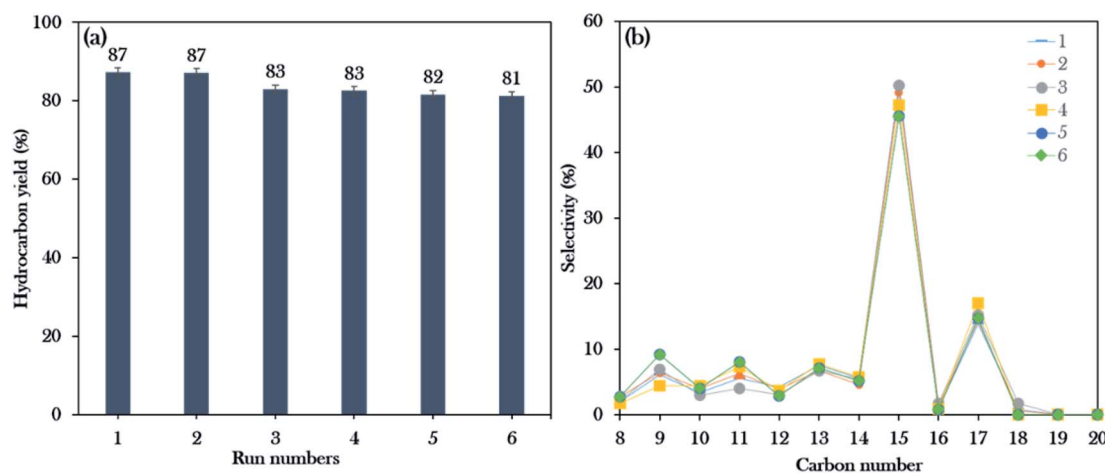

Fig. 10 Reusability studies of the $Ni_{20}La_{20}AC$ catalyst for the 6th run: (a) the hydrocarbon yield profile, (b) hydrocarbon selectivity.

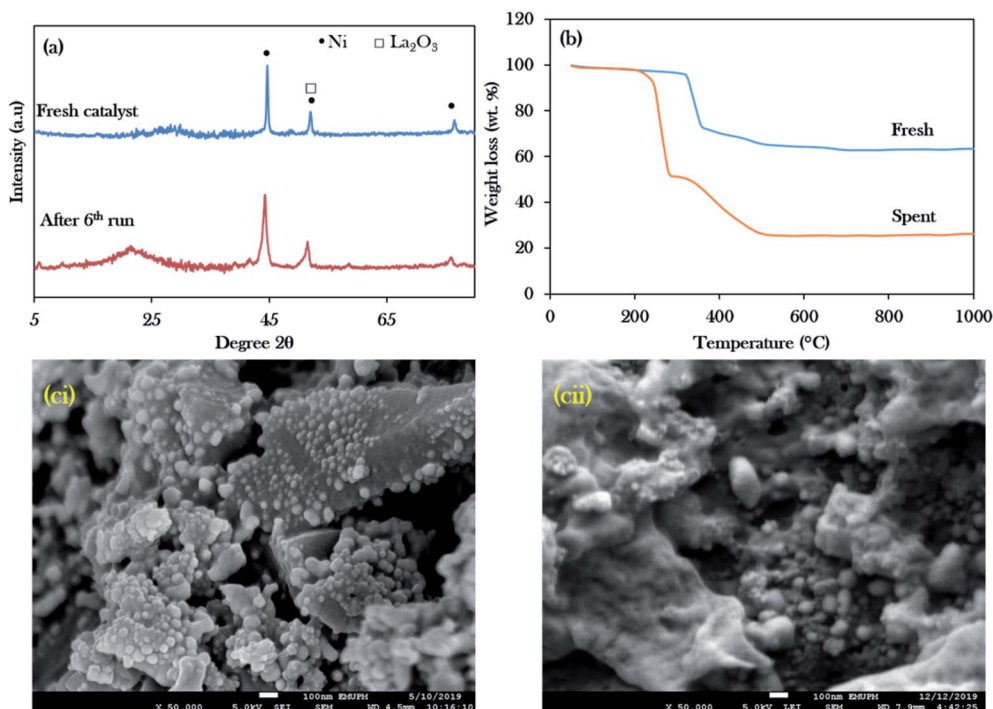**Fig. 11** Stability studies of the $Ni_{20}La_{20}AC$ catalyst for the 6th run: (a) the XRD profile, (b) TGA, (ci) FESEM image for the fresh catalyst, (cii) FESEM image for the spent catalyst.

The amorphous structure of the carbon phase resulted in a weak diffraction peak at $2\theta = 20$–$30°$ in the spent NiLa/AC catalyst, which intensified after deoxygenation, suggesting an increase in the formation of random aromatic carbon sheets. This can be ascribed to the increased amorphous carbon-derived coke. The amount of coke produced was evaluated by TGA analysis as shown in Fig. 11b. It was found that the main decomposition peaks for fresh NiLa/AC catalysts were between 330 °C and 506 °C; however, the spent NiLa/AC catalyst started to decompose at 225 °C to 526 °C. The early decomposition of about 47 wt% ranged from 225 °C to 325 °C, due to the oxidation of the soft coke on the surface.[76] Moreover, it was noted that the spent NiLa/AC catalyst also exhibited the presence of hard coke of about 26 wt%, which decomposed between 330 °C to 750 °C; this revealed that the catalyst surface was covered by coke formation after the deoxygenation reaction.[77] This finding agreed with EDX, which showed a remarkable increment in the C content in the NiLa/AC spent catalyst after 6 deoxygenation runs (Table 5); hence, it strongly implies that the spent NiLa/AC catalyst was masked by the coke.

Fig. 11ci and cii show the electron scanning images of fresh and spent NiLa/AC catalysts; the spent NiLa/AC catalyst was sintered after the reaction. It was expected that the catalysts would be exposed to high temperatures for longer times and would clamp to each other; as a result, the surface area and active sites were reduced and, consequently, deactivation occurred.[78,79] Hence, the majority of the tiny dots in fresh NiLa/AC were enlarged after long-term deoxygenation reactions. This finding, evinced by Kim *et al.*,[80] reported that sintered catalysts typically resulted in reduced catalytic activity due to the loss of

Table 5 Elemental compositions of the fresh NiLa/AC and spent NiLa/AC catalysts

Catalysts	Elemental surface analysis[a]			
	C (wt%)	O (wt%)	Ni (wt%)	La (wt%)
NiLa/AC (fresh)	56.6	19.1	9.0	15.4
NiLa/AC (spent)	69.2	11.7	14.2	4.9

[a] Determined by EDX analysis.

active sites. Even though the NiLa/AC suffered from coke deposits and sintering, the NiLa/AC catalyst still showed consistent deoxygenation activity within 6 consecutive runs without significant reactivity loss, suggesting that the catalyst was highly stable and reusable.

4. Conclusion

The catalytic deoxygenation of WCO *via* deCOx pathways was studied over activated carbon derived-catalysts (NiLa/AC, NiCe/AC, NiFe/AC, NiMn/AC, NiW/AC, and NiZn/AC). Among all the prepared binary metal AC catalysts, the $Ni_{20}La_{20}$/AC catalyst showed very effective deoxygenation performance *via* deCOx reactions and effective exclusivity in producing n-$(C_{15} + C_{17})$ fractions, due to the moderate density of the strongly acidic properties and the low density of the strongly basic properties. The changes in the surface the area had no effect on the formation of n-$(C_{15} + C_{17})$ fractions. In particular, rich La

(20 wt%) and Ni (20 wt%) species led to efficient deoxygenation activity. Based on the OVAT optimization study, about 88% of the hydrocarbon yield and 75% n-$(C_{15} + C_{17})$ selectivity were observed under the favourable conditions: 3 wt% of catalyst loading, 2 h of reaction time, and 350 °C reaction temperature. It also showed excellent stability which was proven by the consistent hydrocarbon yield of over 80%, and over 60% for n-$(C_{15} + C_{17})$ selectivity for 6 consecutive runs.

Conflicts of interest

There are no conflicts of interest to declare.

Acknowledgements

References

1 C. Kordulis, K. Bourikas, M. Gousi, E. Kordouli and A. Lycourghiotis, *Appl. Catal., B*, 2016, **181**, 156–196.

2 K. Treusch, N. Schwaiger, K. Schlackl, R. Nagl, A. Rollett, M. Schadler, B. Hammerschlag, J. Ausserleitner, A. Huber, P. Pucher and M. Siebenhofer, *React. Chem. Eng.*, 2018, **3**, 258–266.

3 E. Santillan-Jimenez and M. Crocker, *J. Chem. Technol. Biotechnol.*, 2012, **87**, 1041–1050.

4 G. Knothe, *Prog. Energy Combust. Sci.*, 2010, **36**, 364–373.

5 R. W. Gosselink, S. A. W. Hollak, S. W. Chang, J. Van Haveren, K. P. De Jong, J. H. Bitter and D. S. Van Es, *ChemSusChem*, 2013, **6**, 1576–1594.

6 R. Shu, R. Li, B. Lin, C. Wang, Z. Cheng and Y. Chen, *Biomass Bioenergy*, 2020, **132**, 105432.

7 P. Kumar, S. R. Yenumala, S. K. Maity and D. Shee, *Appl. Catal., A*, 2014, **471**, 28–38.

8 M. F. Kamaruzaman, Y. H. Taufiq-Yap and D. Derawi, *Biomass Bioenergy*, 2020, **134**, 105476.

9 X. Y. Ooi, W. Gao, H. C. Ong, H. V. Lee, J. C. Juan, W. H. Chen and K. T. Lee, *Renewable Sustainable Energy Rev.*, 2019, **112**, 834–852.

10 S. K. Kim, J. Y. Han, H. Lee, T. Yum, Y. Kim and J. Kim, *Appl. Energy*, 2014, **116**, 199–205.

11 A. N. Kay Lup, F. Abnisa, W. M. A. Wan Daud and M. K. Aroua, *J. Ind. Eng. Chem.*, 2017, **56**, 1–34.

12 K. Jeništová, I. Hachemi, P. Mäki-Arvela, N. Kumar, M. Peurla, L. Capek, J. Wärnå and D. Y. Murzin, *Chem. Eng. J.*, 2017, **316**, 401–409.

13 M. I. Loizides, X. I. Loizidou, D. L. Orthodoxou and D. Petsa, *Recycling*, 2019, 1–10.

14 K. Hanisah, S. Kumar and T. Ay, *J. Environ. Health*, 2013, **4**, 76–81.

15 B. Peng, Q. Shu, J. Wang, G. Wang, D. Wang and M. Han, *Process Saf. Environ. Prot.*, 2008, **86**, 441–447.

16 I. Nikolopoulos, G. Kogkos, E. Kordouli, K. Bourikas, C. Kordulis and A. Lycourghiotis, *Mol. Catal.*, 2020, **482**, 110697.

17 T. Morgan, D. Grubb, E. Santillan-Jimenez and M. Crocker, *Top. Catal.*, 2010, **53**, 820–829.

18 N. Asikin-Mijan, H. V. Lee, G. Abdulkareem-Alsultan, A. Afandi and Y. H. Taufiq-Yap, *J. Cleaner Prod.*, 2017, **167**, 1048–1059.

19 H. Li, H. Ma, W. Zhao, X. Li and J. Long, *Appl. Energy*, 2019, **253**, 113613.

20 S. Thongkumkoon, W. Kiatkittipong, U. Wetwatana, N. Laosiripojana and P. Daorattanachai, *Renewable Energy*, 2019, **140**, 111–123.

21 S. Zulkepli, J. C. Juan, H. V. Lee, N. S. A. Rahman, P. L. Show and E. P. Ng, *Energy Convers. Manage.*, 2018, **165**, 495–508.

22 V. Balasundram, N. Ibrahim, R. M. Kasmani, M. K. A. Hamid, R. Isha, H. Hasbullah and R. R. Ali, *Energy Procedia*, 2017, **142**, 801–808.

23 R. Zhang, Y. Wang and R. C. Brown, *Energy Convers. Manage.*, 2007, **48**, 68–77.

24 G. Wen, Y. Xu, H. Ma, Z. Xu and Z. Tian, *Int. J. Hydrogen Energy*, 2008, **33**, 6657–6666.

25 C. Miao, O. Marin-flores, S. D. Davidson, T. Li, T. Dong, D. Gao, Y. Wang, M. Garcia-pérez and S. Chen, *Fuel*, 2016, **166**, 302–308.

26 J. M. Gómez, M. D. Romero and V. Callejo, *Catal. Today*, 2013, **218–219**, 143–147.

27 N. Asikin-mijan, H. V. Lee, T. S. Marliza and Y. H. Taufiq-Yap, *J. Anal. Appl. Pyrolysis*, 2018, **129**, 221–230.

28 G. Abdulkareem-Alsultan, N. Asikin-mijan, N. Mansir, H. V. Lee, Z. Zainal, A. Islam and Y. H. Taufiq-Yap, *J. Anal. Appl. Pyrolysis*, 2019, **137**, 171–184.

29 X. Cao, L. Li, S. Yu, S. Liu, H. Yu, Q. Wu and A. J. Ragauskas, *J. Anal. Appl. Pyrolysis*, 2019, **138**, 137–144.

30 S. Wang and G. Q. M. Lu, *Appl. Catal., B*, 1998, **19**, 267–277.

31 T. Aysu, N. A. A. Rahman and A. Sanna, *Energy*, 2016, **103**, 205–214.

32 V. Balasundram, N. Ibrahim, R. M. Kasmani, R. Isha, M. K. A. Hamid, R. R. Ali and H. Hasbullah, *Appl. Energy*, 2018, **220**, 787–799.

33 R. Isha and P. T. Williams, *J. Energy Inst.*, 2012, 22–28.

34 M. Akri, S. Pronier, T. Chafik, O. Achak, P. Granger, P. Simon, M. Trentesaux and C. Batiot-dupeyrat, *Appl. Catal., B*, 2017, **205**, 519–531.

35 M. Greluk, M. Rotko and S. Turczyniak-surdacka, *Appl. Catal., A*, 2020, **590**, 117334.

36 P. Osorio-vargas, N. A. Flores-gonzález, R. M. Navarro, J. L. G. Fierro, C. H. Campos and P. Reyes, *Catal. Today*, 2015, **259**, 27–38.

37 N. Asikin-Mijan, H. V. Lee, J. C. Juan, A. R. Noorsaadah, G. Abdulkareem-Alsultan, M. Arumugam and Y. H. Taufiq-Yap, *J. Anal. Appl. Pyrolysis*, 2016, **120**, 110–120.

38 J. Fu, X. Lu and P. E. Savage, *Energy Environ. Sci.*, 2010, **3**, 311–317.

39 M. Jin and M. Choi, *Mol. Catal.*, 2019, **474**, 110419.

40 K. Sun, T. C. Schulz, S. T. Thompson and H. H. Lamb, *Catal. Today*, 2016, **269**, 93–102.

41 G. Abdulkareem-Alsultan, N. Asikin-mijan, H. V. Lee, A. S. Albazzaz and Y. H. Taufiq-Yap, *Energy Convers. Manage.*, 2017, **151**, 311–323.

42 N. Aliana-Nasharuddin, N. Asikin-mijan, G. Abdulkareem-Alsultan, M. I. Saiman, F. A. Alharthi, A. A. Alghamdi and Y. H. Taufiq-Yap, *RSC Adv.*, 2020, **10**, 626–642.

43 N. Asikin-Mijan, J. M. Ooi, G. AbdulKareem-Alsultan, H. V. Lee, M. S. Mastuli, N. Mansir, F. A. Alharthi, A. A. Alghamdi and Y. H. Taufiq-Yap, *J. Cleaner Prod.*, 2020, **249**, 119381.

44 M. S. Gamal, N. Asikin-mijan, M. Arumugam and U. Rashid, *J. Anal. Appl. Pyrolysis*, 2019, **144**, 104690.

45 D. Mukai, S. Tochiya, Y. Murai, M. Imori, T. Hashimoto, Y. Sugiura and Y. Sekine, *Appl. Catal., A*, 2013, **453**, 60–70.

46 J. Chen, H. Zou, Q. Yao, M. Luo, X. Li and Z.-H. Lu, *Appl. Surf. Sci.*, 2020, **501**, 144247.

47 X. Li, B. Yan, S. Yao, S. Kattel, J. G. Chen and T. Wang, *Appl. Catal., B*, 2018, **231**, 213–223.

48 G. Li, F. Zhang, L. Chen, C. Zhang, H. Huang and X. Li, *ChemCatChem*, 2015, **7**, 2646–2653.

49 Y. Zheng, F. Wang, X. Yang, Y. Huang, C. Liu, Z. Zheng and J. Gu, *J. Anal. Appl. Pyrolysis*, 2017, **126**, 169–179.

50 A. Srifa, K. Faungnawakij, V. Itthibenchapong and S. Assabumrungrat, *Chem. Eng. J.*, 2015, **278**, 249–258.

51 V. Balasundram, K. K. Zaman, N. Ibrahim, R. M. Kasmani, R. Isha, M. K. A. Hamid and H. Hasbullah, *J. Anal. Appl. Pyrolysis*, 2018, **134**, 309–325.

52 Y. Zhang, D. Duan, H. Lei, E. Villota and R. Ruan, *Appl. Energy*, 2019, **251**, 113337.

53 C. Tan and W. Tsai, *Int. J. Hydrogen Energy*, 2015, **40**, 14064–14071.

54 R. Ding, Y. Wu, Y. Chen, J. Liang, J. Liu and M. Yang, *Chem. Eng. Sci.*, 2015, **135**, 517–525.

55 B. C. Ang, I. I. Yaacob and I. Nurdin, *J. Nanomater.*, 2013, **2013**, 1–6.

56 S. Janampelli and S. Darbha, *Mol. Catal.*, 2018, **451**, 125–134.

57 G. U. O. Haiyan, M. A. Lunjie, S. Fei, Y. Gang, Z. Yanzong, D. Shihuai, Z. Jing, S. Chun and Z. Yongmei, *J. Rare Earths*, 2017, **35**, 593–601.

58 W. Li, K. Yang, J. Peng, L. Zhang, S. Guo and H. Xia, *Ind. Crops Prod.*, 2008, **28**, 190–198.

59 J. Jeong, H. W. Lee, S. H. Jang, S. Ryu, Y. Kim, R. Park, S.-C. Jung, J.-K. Jeon and Y.-K. Park, *Catalysts*, 2019, **9**, 1–11.

60 M. Roussel, S. Norsic, J.-L. Lemberton, M. Guisnet, T. Cseri and E. Benazzi, *Appl. Catal., A*, 2005, **279**, 53–58.

61 M. Gousi, E. Kordouli, K. Bourikas, E. Simianakis, S. Ladas, G. D. Panagiotou, C. Kordulis and A. Lycourghiotis, *Catal. Today*, DOI: 10.1016/j.cattod.2019.02.034.

62 F. A. A. Twaiq, A. R. Mohamad and S. Bhatia, *Fuel Process. Technol.*, 2004, **85**, 1283–1300.

63 E. W. Qian, N. Chen and S. Gong, *J. Mol. Catal. A: Chem.*, 2014, **387**, 76–85.

64 M. Renz, *Eur. J. Org. Chem.*, 2005, 979–988.

65 M. Tamura, T. Tonomura, K. Shimizu and A. Satsuma, *Green Chem.*, 2012, **14**, 984–991.

66 X. Li, X. Zhang, S. Shao, L. Dong, J. Zhang, C. Hu and Y. Cai, *Bioresour. Technol.*, 2018, **259**, 191–197.

67 G. Abdulkareem-Alsultan, N. Asikin-Mijan, G. Mustafa-Alsultan, H. V. Lee, K. Wilson and Y. H. Taufiq-Yap, *R. Soc. Chem.*, 2020, **10**, 4996–5009.

68 J. K. Satyarthi and D. Srinivas, *Energy Fuels*, 2011, **25**, 3318–3322.

69 H. K. G. Singh, S. Yusup, A. T. Quitain, B. Abdullah, M. Ameen, M. Sasaki, T. Kida and K. W. Cheah, *Environ. Res.*, 2020, **186**, 109616.

70 L. Hermida, A. Z. Abdullah and A. R. Mohamed, *Renewable Sustainable Energy Rev.*, 2015, **42**, 1223–1233.

71 I. Kim, A. A. Dwiatmoko, J. Choi, D. J. Suh, J. Jae, J. Ha and J. Kim, *J. Ind. Eng. Chem.*, 2017, **56**, 74–81.

72 A. Bohre, M. I. Alam, K. Avasthi, F. Ruiz-Zepeda and B. Likozar, *Appl. Catal., B*, 2020, **276**, 119069.

73 Y. Lou, P. He, L. Zhao and H. Song, *Fuel*, 2016, **183**, 396–404.

74 M. Snåre, I. Kubičková, P. Mäki-Arvela, D. Chichova, K. Eränen and D. Y. Murzin, *Fuel*, 2008, **87**, 933–945.

75 H. Bernas, K. Eränen, I. Simakova, A. Leino, K. Kordás, J. Myllyoja, P. Mäki-arvela, T. Salmi and D. Y. Murzin, *Fuel*, 2010, **89**, 2033–2039.

76 N. Taufiqurrahmi, A. R. Mohamed and S. Bhatia, *Chem. Eng. J.*, 2010, **163**, 413–421.

77 S. K. Sahoo, S. S. Ray and I. D. Singh, *Appl. Catal., A*, 2004, **278**, 83–91.

78 V. G. D. la Cruz-Flores, A. Martinez-Hernandez and M. A. Gracia-Pinilla, *Appl. Catal., A*, 2020, **594**, 117455.

79 J. Sehested, J. A. P. Gelten and S. Helveg, *Appl. Catal., A*, 2006, **309**, 237–246.

80 S. Kim, E. E. Kwon, Y. T. Kim, S. Jung, H. J. Kim, G. W. Huber and J. Lee, *Green Chem.*, 2019, **21**, 3715–3743.